Chinese Journal of Natural Medicines

Facilitating microglial phagocytosis by which Jiawei Xionggui Decoction alleviates cognitive impairment *via* TREM2–mediated energy metabolic reprogramming

Wen Wen, Jie Chen, Junbao Xiang, Shiqi Zhang, Jingru Liu, Jie Wang, Ping Wang, Shijun Xu

Citation: Wen Wen, Jie Chen, Junbao Xiang, Shiqi Zhang, Jingru Liu, Jie Wang, Ping Wang, Shijun Xu, Facilitating microglial phagocytosis by which Jiawei Xionggui Decoction alleviates cognitive impairment *via* TREM2–mediated energy metabolic reprogramming, Chinese Journal of Natural Medicines, 2025, 23(8), 909–919. doi: 10.1016/S1875–5364(25)60927–7.

View online: https://doi.org/10.1016/S1875–5364(25)60927–7

Chinese Journal of Natural Medicines 23 (2025) 909-919

Contents lists available at ScienceDirect

Chinese Journal of Natural Medicines

journal homepage: www.cjnmcpu.com/

Original article

Facilitating microglial phagocytosis by which Jiawei Xionggui Decoction alleviates cognitive impairment *via* TREM2-mediated energy metabolic reprogramming

Wen Wen[a,b,c], Jie Chen[a,b,c], Junbao Xiang[a,b,c], Shiqi Zhang[a,b,c], Jingru Liu[d], Jie Wang[a,b,c], Ping Wang[a,b,c,*], Shijun Xu[a,b,c,*]

[a] *State Key Laboratory of Southwestern Chinese Medicine Resources, Chengdu University of Traditional Chinese Medicine, Chengdu 611137, China*
[b] *School of Pharmacy, Chengdu University of Traditional Chinese Medicine, Chengdu 611137, China*
[c] *Institute of Material Medica Integration and Transformation for Brain Disorders, Chengdu University of Traditional Chinese Medicine, Chengdu 611137, China*
[d] *Division of Biosciences, University College London, London WC1E6BT, UK*

ARTICLE INFO

Article history:
Received 6 September 2024
Revised 21 December 2024
Accepted 26 February 2025
Available online 20 August 2025

Keywords:
Akt/mTOR/HIF-1α
Energy metabolic reprogramming
Jiawei Xionggui Decoction
Microglial phagocytosis
Triggering receptor expressed on myeloid cells 2 (TREM2)

ABSTRACT

Triggering receptor expressed on myeloid cells 2 (TREM2)-mediated microglial phagocytosis is an energy-intensive process that plays a crucial role in amyloid beta (Aβ) clearance in Alzheimer's disease (AD). Energy metabolic reprogramming (EMR) in microglia induced by TREM2 presents therapeutic targets for cognitive impairment in AD. Jiawei Xionggui Decoction (JWXG) has demonstrated effectiveness in enhancing energy supply, protecting microglia, and mitigating cognitive impairment in APP/PS1 mice. However, the mechanism by which JWXG enhances Aβ phagocytosis through TREM2-mediated EMR in microglia remains unclear. This study investigates how JWXG facilitates microglial phagocytosis and alleviates cognitive deficits in AD through TREM2-mediated EMR. Microglial phagocytosis was evaluated through immunofluorescence staining *in vitro* and *in vivo*. The EMR level of microglia was assessed using high-performance liquid chromatography (HPLC) and enzyme-linked immunosorbent assay (ELISA) kits. The TREM2/protein kinase B (Akt)/mammalian target of rapamycin (mTOR)/hypoxia-inducible factor-1α (HIF-1α) signaling pathway was analyzed using Western blotting in BV_2 cells. $TREM2^{-/-}$ BV_2 cells were utilized for reverse validation experiments. The Aβ burden, neuropathological features, and cognitive ability in APP/PS1 mice were evaluated using ELISA kits, immunohistochemistry (IHC), and the Morris water maze (MWM) test. JWXG enhanced both the phagocytosis of EMR disorder-BV_2 cells (EMRD-BV_2) and increased EMR levels. Notably, these effects were significantly reversed in $TREM2^{-/-}$ BV_2 cells. JWXG elevated TREM2 expression, adenosine triphosphate (ATP) levels, and microglial phagocytosis in APP/PS1 mice. Additionally, JWXG reduced Aβ-burden, neuropathological lesions, and cognitive deficits in APP/PS1 mice. In conclusion, JWXG promoted TREM2-induced EMR and enhanced microglial phagocytosis, thereby reducing Aβ deposition, improving neuropathological lesions, and alleviating cognitive deficits.

1. Introduction

Amyloid beta (Aβ) accumulation and its associated neurotoxicity represent critical factors in the neurological deterioration observed in Alzheimer's disease (AD). The enhancement of Aβ clearance has emerged as a primary strategy in drug development, with several monoclonal antibodies receiving Food and Drug Administration (FDA) approval for AD treatment, including aducanumab and lecanemab [1-3]. These developments demonstrate that facilitating Aβ removal effectively improves cognitive impairment in AD. Microglial phagocytosis, performed by the brain's exclusive immune cells, presents a distinct target for Aβ clearance [1, 4-7], though effective therapeutic interventions remain unavailable.

Triggering receptor expressed on myeloid cells 2 (TREM2), a significant risk gene in AD, is predominantly expressed in brain microglia and plays a crucial role in microglial functions, including phagocytosis, energy metabolism, and survival [8]. TREM2 enhances microglial activation and phagocytosis through mammalian target of rapamycin (mTOR) pathway stimulation [9]. Additionally, Aβ functions as a TREM2 ligand, binding directly to its extracellular domain. Acute Aβ administration triggers TREM2-mediated activation of the protein kinase B (Akt)/mTOR/hypoxia-inducible factor-1α (HIF-1α) signaling pathway [10]. HIF-1α serves as a key transcriptional regulator of glycolysis by modulating the expression and activity of glucose metabolism-related enzymes [11]. This process initiates microglial energy metabolic reprogramming (EMR) from oxidative phosphorylation (OXPHOS) to glycolysis, essential for maintaining microglial phagocytosis [12, 13], a phenomenon known as the Warburg effect. The Akt/mTOR/HIF-

* Corresponding author.
E-mail addresses: viviansector@aliyun.com (P. Wang); xushijun@cdutcm.edu.cn (S. Xu)

https://doi.org/10.1016/S1875-5364(25)60927-7

1α pathway represents a well-established signaling mechanism for EMR [12, 14]. Prolonged or repeated Aβ exposure leads to overall microglial energy metabolism deficiency, resulting in reduced or absent Akt/mTOR/HIF-1α pathway responsiveness, thereby inhibiting microglial EMR, a condition termed microglial immune tolerance [15, 16]. This tolerance exacerbates microglial phagocytic dysfunction and impairs Aβ clearance, leading to excessive Aβ accumulation and subsequent cognitive decline [17]. Recent research demonstrates that ATV/TREM2 (an agonistic anti-TREM2 antibody) improves energy metabolism and microglial phagocytosis in Alzheimer's disease models *in vivo* and *in vitro* [18, 19]. These findings suggest that enhancing microglial phagocytosis through EMR promotion represents an effective strategy for addressing AD-related cognitive impairment.

Numerous studies have demonstrated that traditional Chinese medicine (TCM) shows significant potential in developing new treatments for AD [20-22]. Research confirms that TCM can mitigate cognitive dysfunction and neuronal damage in AD models by enhancing microglial phagocytosis, as evidenced by studies on *Dctionracaena cochinchinensis* stemwood, Juzen Taihoto and Shiquan Dabu Formula [23-25]. Jiawei Xionggui Decoction (JWXG), a classic formula derived from *Wan Shi Nv Ke*, comprises Chuanxiong Rhizoma (the rhizoma and root of *Ligusticum chuanxiong*), Scutellariae Radix (the radix of *Scutellaria baicalensis*), and Angelica Sinensis Radix (the radix of *Angelica sinensis*). Its composition ratio and application for cognitive impairment improvement have received patent authorization in China (Invention Patent Authorisation No. ZL201310132096.2). Previous studies demonstrate that JWXG enhances cognitive function, decreases Aβ burden, and inhibits microglial inflammatory response in AD model mice [26-28]. Furthermore, JWXG enhances brain energy metabolism in APP/PS1 mice and multiple infarct dementia rats while modulating lactate content by facilitating monocarboxylate transporter-1 and monocarboxylate transporter-2 expression in multiple infarct dementia rats [29-32]. Additionally, chlorogenic acid, an active constituent of JWXG, activates the mTOR/HIF-1α signaling pathway [33], the primary pathway regulating EMR. Research indicates that JWXG-derived active ingredients, including baicalin, baicalein, chlorogenic acid, and ferulic acid, effectively reduce cognitive deficits in AD models [34-39]. Notably, baicalin and ferulic acid serve as quality control indices for *Ligusticum chuanxiong*, *Scutellaria baicalensis* and *Angelica sinensis* required in the *Chinese Pharmacopoeia 2020*. Thus, their contents were utilized to assess JWXG quality in this study. This investigation employed 6-month-old (6-mo) transgenic APP/PS1 mice, transgenic TREM2$^{-/-}$-BV_2 cells, and amyloid-β oligomers (oAβ)-induced EMR disorder-BV_2 (EMRD-BV_2) to elucidate JWXG's therapeutic effects and underlying mechanisms in reducing AD cognitive deficits, particularly focusing on TREM2-mediated microglial phagocytosis and EMR.

2. Material and methods

2.1. JWXG preparation

Chuanxiong Rhizoma (Batch No. 2020088) and Scutellariae Radix (Batch No. 2020001) were obtained from Sichuan NEAUTUS Traditional Chinese Medicine Co., Ltd. (Chengdu, China); Angelicae Sinensis Radix (Batch No. 202001) was provided by Chengdu Ji'an Kang Medicine Industry Co., Ltd. (Chengdu, China). These herbs were authenticated by Prof. Yuntong Ma (Chengdu University of Traditional Chinese Medicine, Chengdu, China). The JWXG preparation involved boiling 15 g Chuanxiong Rhizoma, 9 g Scutellariae Radix, and 3 g Angelicae Sinensis Radix twice in 250 mL of water, followed by filtration and mixing. The decoction was concentrated under vacuum with a rotary evaporator to 0.45 g·mL^{-1} for content determination. The liquid extract underwent low-temperature vacuum freeze-drying (−80 °C) to produce freeze-dried powder, which was stored in a dryer. The clinical JWXG dosage is 27 g daily for patients. The mice clinical equivalent dosage was calculated based on kg mice/human body weight using a conversion ratio of 9 times, as documented in *Experimental Pharmacology*. Consequently, the daily JWXG dosage for mice was established at 4.05 g·kg^{-1} in this study.

2.2. High-performance liquid chromatography (HPLC) analysis

After filtration through a 0.22 μm microporous membrane and dilution to 1∶100, an Agilent 1260 liquid chromatograph system (Agilent, USA) and Q Exactive liquid chromatography-tandem mass spectrometry (LC-MS/MS) (Thermo Fisher, USA) were utilized to analyze baicalin, baicalein, ferulic acid and chlorogenic acid in JWXG according to the *Chinese Pharmacopoeia 2020* method for *Ligusticum chuanxiong*, *Scutellaria baicalensis* and *Angelica sinensis*. The compounds were separated using a Poroshell 120 Energy charge (EC)-C_{18} (4.6 mm × 100 mm, 2.7 μm, Agilent, USA) chromatographic column. The elution gradient consisted of purified 0.1% aqueous formic acid (A) and 0.1% acetonitrile formate solution (B). Gradient elution proceeded according to the following program: 0→20 min, 95%→5% A. The column temperature and injection volume were set to 30 °C and 1 μL, respectively. Quantification was performed by multiple reaction monitoring mode with transitions of *m/z* 290.988→123.054→32.17 for baicalin (+), *m/z* 447.088→123.071→54.03 for baicalein (+), *m/z* 193.05→134.071→14.86 for ferulic acid (−), *m/z* 353.125→84.982→39.63 for chlorogenic acid (−). Other main working parameters were set as usual.

2.3. Cell culture, lentivirus infection and stimulation

The lentivirus target virus [TREM2-short hairpin ribonucleic acid (shRNA)] and an equivalent control virus were used to treat BV_2 cells. After 72-h stimulation, unsuccessfully infected BV_2 cells were eliminated using 5 μg·mL^{-1} of puromycin to obtain stable shTREM2-BV_2 and GFP-BV_2 cells. $Aβ_{25-35}$ peptides (Chinese peptide) were dissolved in HFIP (RHAWN) at a final concentration of 1 mmol·L^{-1}, followed by HFIP evaporation to collect Aβ peptide and storage at −80 °C. oAβ was prepared by dissolving $Aβ_{25-35}$ peptides to 100 μmol·L^{-1} in Dulbecco's modified Eagle medium (DMEM), followed by overnight incubation at 4 °C. BV_2 cells were obtained from the Institute of Basic Medical Sciences, Chinese Academy of Medical Sciences (Identification No. 1101MOUPUMC000063). BV_2 cells were cultured in basic DMEM containing 10% FBS and 1% P/S and stimulated with either vehicle (DMEM containing 0.5% FBS to prevent cell death), 2 μmol·L^{-1} oAβ, or 2 μmol·L^{-1} oAβ + JWXG at varying concentrations for 24 h. In specific experiments, BV_2 cells were pre-treated with 5 mmol·L^{-1} 2-DG for 1 h to inhibit glycolysis. The experiments employed a tolerant model simulating prolonged conditions, where cells were exposed to vehicle or oAβ (2 μmol·L^{-1}) for 24 h, washed with phosphate-buffered saline (PBS), and further cultured in vehicle DMEM for 3−5 d. Subsequently, the cells were re-stimulated with oAβ (2 μmol·L^{-1}), 2 μmol·L^{-1} oAβ + JWXG at different concentrations, or incubated with a vehicle for 24 h (Fig. 1).

2.4. Phagocytosis assay

The phagocytosis assay was performed according to previously described methods [40]. Briefly, BV_2 cells were incubated at a density of 30 000/well in 12-well plates. Following re-stimulation with oAβ (2 μmol·L^{-1}) or alternative stimuli, pre-opsonized fluorescent latex beads (50% PBS + 50% FBS, FL-PS-G-01 DaE

Technology, Tianjin, China) were added to the wells at a density of 50 beads/cell and incubated at 37 °C for 4 h. After gentle washing to remove non-phagocytosed beads, the cells were fixed with 4% PFA at room temperature. Images were captured using a fluorescent microscope, and phagocytosed beads were counted.

2.5. Glycolysis measurements

EC assays were conducted according to the previously reported protocol, and the levels of adenosine triphosphate (ATP), adenosine diphosphate (ADP), and adenosine monophosphate (AMP) were determined using the standard curve [27]. EC was calculated using the following formula:

$$EC = \frac{[ATP] + 0.5 \times [ADP]}{[ATP] + [ADP] + [AMP]}$$

Pyruvate kinase (PK), fructose-6-phosphate kinase (F-6-PK), and hexokinase (HK) activity tests were performed to evaluate the level of EMR in BV_2 cells, following the standard protocols specified in the PK, F-6-PK, and HK activity kit instructions (Suzhou Grace Biotechnology Co., Ltd., Suzhou, China). The intracellular content of lactate and pyruvate in BV_2 cells was measured to determine the ratio between cellular glycolysis and tricarboxylic acid cycle, following the standard protocols specified in the lactate and pyruvate content kit instructions (Nanjing JianCheng Bioengineering Institute Co., Ltd., Nanjing, China).

2.6. Real-time quantitative polymerase chain reaction (RT-qPCR)

Total RNA was extracted using Total RNA Isolation Kits (#R220901, Foregene). cDNA synthesis was performed using a SweScript All-in-One RT SuperMix kit (#G3337-50, ServiceBio). RT-qPCR analysis was conducted using SYBR Green mix (#G3326-05, ServiceBio) with the following primer pairs: *MM-CD68*: 5'-CTC TCT AAG GCT ACA GGC TGC T-3' (forward) and 5'-TCA CGG TTG CAA GAG AAA CA-3' (reverse); *MM-TREM2*: 5'-TAC TGG TGG AGG TGC TGG AG-3' (forward) and 5'-AGG ATG AAA CCT GCC TGG AG-3' (reverse); *MM-β-actin*: 5'-GCT CCG GCA TGT GCA AAG-3' (forward) and 5'-TTC CCA CCA TCA CAC CCT GG-3' (reverse). The relative expression of target gene messenger RNA (mRNA) was analyzed according to a standard procedure [12].

2.7. Western blotting

Western blotting was performed following a standard protocol [41]. Briefly, the denatured target proteins were separated using SDS-PAGE, transferred to PVDF membranes, and blocked in a blocking solution (5% skimmed milk dissolved in TBST). Primary antibodies including rabbit anti-HIF-1α (#36169S, CST, MA, USA), rabbit anti-TREM2 (#bs-2723R, Bioss, Beijing, China), rabbit anti-phosphorylated (p)-mTOR (Ser 2448, #5536T, CST), rabbit anti-mTOR (#2983S, CST), rabbit anti-p-Akt (Ser473, #4060S, CST), rabbit anti-Akt (#4685S, CST), and rabbit anti-*β*-actin (#GB12001, Servicebio, Wuhan, China) were applied at a dilution ratio of 1∶1000 for 12 h at 4 °C. Subsequently, horseradish peroxidase (HRP)-conjugated secondary antibody was applied for 2 h at room temperature. The membranes were analyzed using a chemiluminescence reagent and quantified using a chemiluminescent detection software system (ChampChemi 610 Plus, Beijing Sage Creation Science Co., Ltd., Beijing, China) and analyzed using quantity one software.

2.8. Animals and treatment

The experimental protocols were approved by the Animal Care and Use Committee of the Institute of Material Medica Integration and Transformation for Brain Disorders (No. IBD 20200010). 3-mo APP/PS1 mice were acquired from Beijing HFK Bio-Technology Co., Ltd., Beijing, China (Certificate No. 1103222011009531), while C57BL/6J mice were obtained from Hunan SJA Laboratory Animal Co., Ltd., Changsha, China (Certificate No. 1107272011006639). All mice received unrestricted access to food and water in a specific pathogen-free (SPF) facility at Chengdu University of TCM. All experimental procedures strictly adhered to the guidelines of the National Institutes of Health (NIH, USA). Following three months of domestication and adaptive feeding, APP/PS1 mice (JWXG group) received daily oral administration of JWXG for three months, while C57BL/6J mice and the APP/PS1 group received an equal volume of 0.9% saline. Subsequently, mice underwent a Morris water maze (MWM) test following a standard protocol [42]. After the MWM test, animals were anesthetized with 40 mg·kg^{-1} sodium pentobarbital saline solution (#69020100, i.p., Merck, Darmstadt, Germany). The mouse brain tissue underwent transcranial perfusion with pre-cooled normal saline and was collected after euthanasia. The right hemisphere was preserved in liquid nitrogen for Western blotting, RT-qPCR, and enzyme-linked immunosorbent assay (ELISA) kit analysis, while the left hemisphere was fixed with 4% paraformaldehyde (G1101, Service Bio., Wuhan, China) for morphological analysis (Fig. 1).

2.9. MWM test

The Noldus mice MWM was utilized to assess spatial learning and memory capabilities in mice (Noldus Information Technology, Wageningen, Netherlands). An escape platform (diameter, 4.5 cm) was positioned 1 cm below the water surface. During testing, animals were required to locate the hidden escape platform within 60 s. If unsuccessful, the animal was guided to the platform for 10 s at test completion. The assessment spanned 6 d,

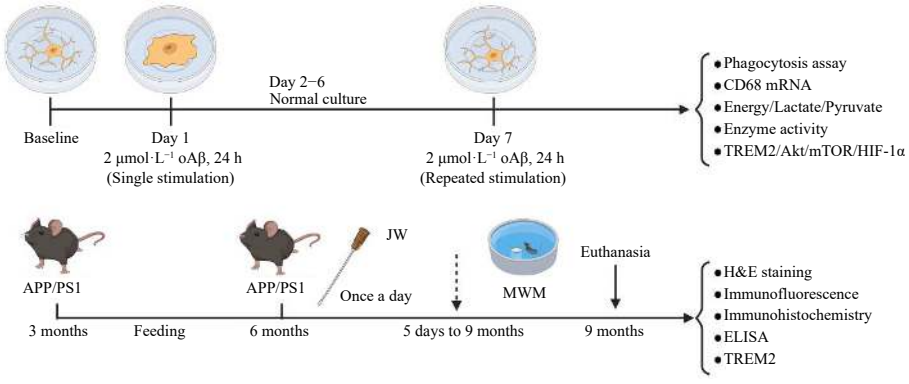

Fig. 1 The experimental flow chart of this work *in vitro* and *in vivo*.

comprising 5 training days and a partial probe trial on day 6 without the platform. On the final day, animals underwent a single probe test without the platform. The escape latency, time to reach the platform or platform zone, duration in the platform or platform zone, and frequency of crossing the platform or platform zone were measured to assess learning and memory capacity.

2.10. Detection of $A\beta_{1-40}$/$A\beta_{1-42}$ and lactic acid of brain tissue

The ELISA kits of $A\beta_{1-40}$ and $A\beta_{1-42}$ were employed to quantify the levels of $A\beta_{1-40}$ and $A\beta_{1-42}$ in brain tissue. Following the manufacturer's instructions (Elabscience Biotechnology Co., Ltd., Wuhan, China), brain samples were prepared by grinding with PBS. After completing a standard protocol, the OD value was measured at 450 nm following 30 min incubation using the Multiskan spectrum spectrophotometer.

Mouse brain tissue (20 mg) was ground on ice with pure water, and the supernatant was collected after ultrasonic crushing and centrifugation. This procedure was repeated twice. All supernatant fractions were concentrated under vacuum using a rotary evaporator. The samples were prepared, and lactic acid was analyzed according to the previously described protocol [43].

2.11. Hematoxylin and eosin (H&E), IHC, and immunofluorescence (IF) staining

H&E staining was performed to evaluate neuronal damage in the cortex and hippocampus of mice, as previously reported [39]. Brain tissue sections (4 μm) were dewaxed with xylene and stained, followed by visualization of each stained slice. IHC and IF analyses followed standard protocols [42, 44]. The 4-μm brain tissue sections underwent baking, rehydration, antigen retrieval, and peroxide blocking before overnight incubation at 4 °C with mouse anti-*β*-amyloid (1∶500, #15126, CST, MA, USA), mouse anti-AT8 (1∶500, #MN1020, Thermo Fisher, MA, USA), and rabbit anti-Iba1 (1∶500, #GB113502-100, Servicebio, Wuhan, China). Subsequently, sections were treated with HRP-conjugated secondary antibody, Cy3 anti-rabbit secondary antibody (1∶300), or 488 anti-mouse secondary antibody (1∶300) for 2 h at RT. IHC sections were developed using a DAB kit (#AR1022, BOSTER, Wuhan, China) and counterstained with nuclear hematoxylin. IF sections were counterstained with DAPI solution (2 μg·mL^{-1}, #G1012, Servicebio, Wuhan, China). IHC sections were analyzed using ImageJ. For microglia quantification around Aβ, Iba1 positive cells within 20 μm of Aβ plaques were manually counted.

2.12. Statistical analysis

ImageJ software was employed for quantitative analysis of H&E, IHC, and IF images, while Quantity One software was used for quantifying Western blotting bands. All results were expressed as mean ± SEM and analyzed using the R language. Double-factor variance analysis was conducted to evaluate escape latency in the MWM test. Differences between groups were assessed using one-way analysis of variance. Statistical significance was established at $P < 0.05$.

3. Results

3.1. The content of active component in JWXG

LC-MS/MS methodology was utilized to quantify the content of chlorogenic acid, ferulic acid, baicalin, and baicalein, with all four active ingredients detected in JWXG. Based on the standard curve ($R^2 > 0.99$), their respective contents in JWXG were determined to be 7.96, 1.66, 65.59, and 123.90 μg·mL^{-1} (see Supporting information).

3.2. JWXG enhanced microglial phagocytosis in EMRD-BV_2 cells and in APP/PS1 mice

As CD68 serves as a marker of microglial phagocytosis, the expression of *CD68* mRNA was initially measured to assess JWXG's phagocytosis-promoting effect in BV_2 cells under different energy metabolic states. Compared to BV_2 cells, the *CD68* mRNA level in EMR-BV_2 cells (oAβ acute stimulation) showed significant elevation (Fig. 2A, $P < 0.01$), while its expression remained unchanged in EMRD-BV_2 cells (repeatedly stimulated by oAβ) (Fig. 2B, $P > 0.05$), suggesting that oAβ reduplicative stimulation-induced EMRD inhibited microglial phagocytosis. Notably, JWXG significantly enhanced the expression of *CD68* mRNA in EMRD-BV_2 cells in a dose-dependent manner (Fig. 2B, $P < 0.05$). Consistent with *CD68* mRNA expression, JWXG significantly increased the number of fluorescent latex beads within EMRD-BV_2 cells in a dose-dependent pattern (Figs. 2C and 2D, $P < 0.05$ or $P < 0.01$). These observations indicate that JWXG enhances microglial phagocytosis ability in EMRD-BV_2 cells. As anticipated, the ratio of Iba1$^+$ microglia to Aβ plaques was significantly higher in JWXG mice compared to APP/PS1 mice, accompanied by substantial microglial accumulation around Aβ plaques (Figs. 2E and 2F, $P < 0.05$). Additionally, the *CD68* mRNA expression in brain tissue showed no significant difference between C57BL/6J and APP/PS1 mice but was markedly elevated following JWXG administration (Fig. 2G, $P < 0.01$). These findings demonstrate that JWXG enhances microglial phagocytosis both *in vitro* and *in vivo*.

3.3. JWXG increased energy production by enhancing EMR in vitro and in vivo

Brain energy deficiency is a well-documented pathological feature in Alzheimer's disease (AD) and associated animal models, largely due to a metabolic shift from efficient mitochondrial respiration to less efficient glycolysis [45-48]. To assess the potential of JWXG in restoring cellular energy under energy-restricted conditions, we examined its effects on BV_2 microglial cells subjected to EMRD. No significant difference in EC levels was observed between normal BV_2 and EMRD-BV_2 cells; however, JWXG treatment led to a dose-dependent increase in EC levels in EMRD-BV_2 cells (Fig. 3A, $P < 0.05$). Lactic acid, pyruvate, and the lactic acid/pyruvate ratio—key metabolic indicators of glycolytic activity—also showed no baseline differences between BV_2 and EMRD-BV_2 cells. Nevertheless, all three parameters were significantly elevated following JWXG administration in EMRD-BV_2 cells (Fig. 3B–3D, $P < 0.05$ or $P < 0.01$). the activities of the glycolytic rate-limiting enzymes HK, PFK, and PK did not differ between BV_2 and EMRD-BV_2 cells at baseline but were significantly increased in a dose-dependent manner by JWXG in EMRD-BV_2 cells (Figs. 3E–3G, $P > 0.05$). These enhancements were effectively reversed by 2-DG, a glycolytic inhibitor targeting HK, with the exception of HK activity, which remained elevated. *In vivo*, the brain EC level in APP/PS1 transgenic mice was significantly reduced compared with wild-type C57BL/6J mice, but was markedly restored after JWXG treatment (Fig. 3H, $P < 0.05$ or $P < 0.01$). Correspondingly, brain lactic acid levels were significantly higher in JWXG-treated APP/PS1 mice compared to untreated counterparts (Fig. 3I). These findings suggest that JWXG promotes energy production in both *in vitro* and *in vivo* models by enhancing glycolytic metabolism.

3.4. JWXG promoted microglial phagocytosis through TREM2-mediated Akt/mTOR/HIF-1α pathway

The Akt/mTOR/HIF-1α pathway represents a crucial mech-

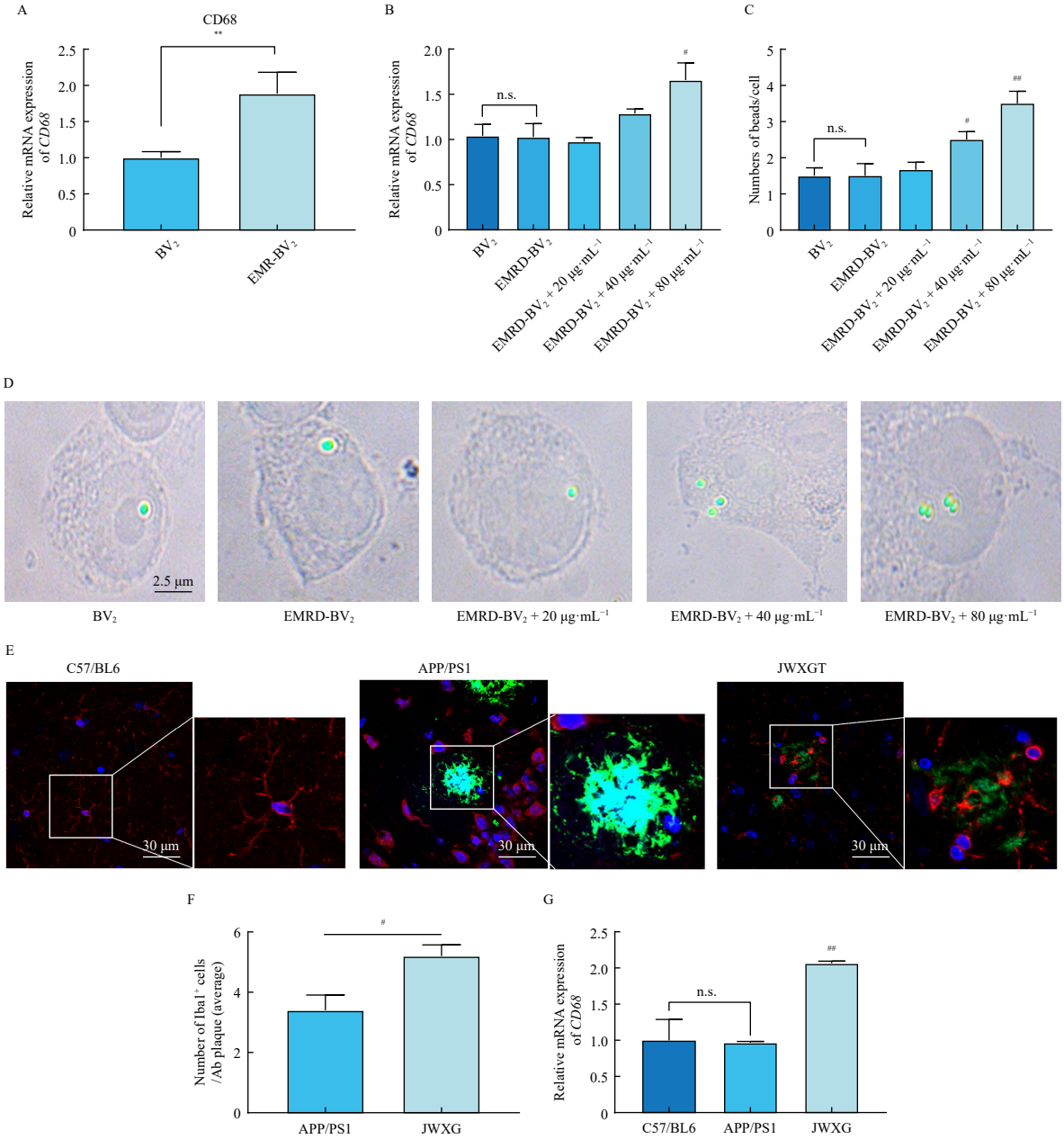

Fig. 2 JWXG enhanced phagocytosis of EMRD-BV_2 and microglia in APP/PS1 mice. (A, B) *CD68* mRNA levels *in vitro* (n = 6). (C) Quantification of internalized fluorescent latex beads *in vitro* (n = 6). (D) Representative images of phagocytosed fluorescent latex beads *in vitro*. (E) Immunofluorescence images showing colocalization of Iba1$^+$ microglia (red), Aβ plaques (green), and nuclei (DAPI, blue) in the cortex of mice. (F) Quantification of Iba1$^+$ microglia colocalized with Aβ plaques in APP/PS1 mice (n = 3). (G) *CD68* mRNA level of mice (n = 3). The data are expressed as mean ± SEM. $^*P < 0.05$, $^{**}P < 0.01$ *vs* BV_2 cells or C57BL/6J mice; $^{\#}P < 0.05$, $^{\#\#}P < 0.01$ *vs* EMRD-BV_2 cells or APP/PS1 mice; n.s. means no significant differences.

anism in EMR-associated microglial phagocytosis [12]. Initially, the ratios of p-Akt/Akt, p-mTOR/mTOR, and HIF-1α/β-actin showed no significant differences between EMRD-BV_2 cells and BV_2 cells. However, these ratios significantly increased in EMRD-BV_2 cells following JWXG treatment (Figs. 4A–4D, $P < 0.05$). Additionally, TREM2 expression levels were significantly elevated in JWXG groups compared to EMRD-BV_2 cells and APP/PS1 mice (Figs. 4E–4J, $P < 0.05$ or $P < 0.01$). TREM2, functioning as a transmembrane promotor of microglial phagocytosis located in the microglial membrane, was knocked down in shTREM2-BV_2 cells using lentivirus, with verification through fluorescence and RT-qPCR (Fig. S1). Notably, TREM2 knockdown partially reversed JWXG's effects on microglial phagocytosis enhancement, glycolysis-mediated energy production improvement, and Akt/mTOR/HIF-1α pathway activation in EMRD-BV_2 cells (Figs. 5A–5N, $P < 0.05$). These findings suggest that JWXG enhances microglial phagocytosis through activation of the TREM2-mediated Akt/mTOR/HIF-1α pathway and EMR enhancement.

3.5. JWXG attenuated Aβ burden and neuronal damage in APP/PS1 mice

Microglial phagocytosis serves a crucial function in eliminating toxic proteins, including Aβ, from the brain. The Aβ staining results revealed that Aβ$^+$ plaques in the cerebral cortex and hippocampus of APP/PS1 mice were significantly elevated compared to C57BL/6J mice but decreased in JWXG-treated mice relative to APP/PS1 mice (Figs. 6A–6C, $P < 0.01$). JWXG's effects on $Aβ_{1-40}$ and $Aβ_{1-42}$ levels in APP/PS1 mice brain tissues closely paralleled the Aβ staining findings (Figs. 6D and 6E, $P < 0.05$ or $P < 0.01$). Neuronal impairment represents a characteristic manifestation of Aβ neurotoxicity [49]. The data demonstrated neuronal injury features in APP/PS1 mice cortex and hippocampus regions, including cortical thinning, neuronal atrophy, and neuron-

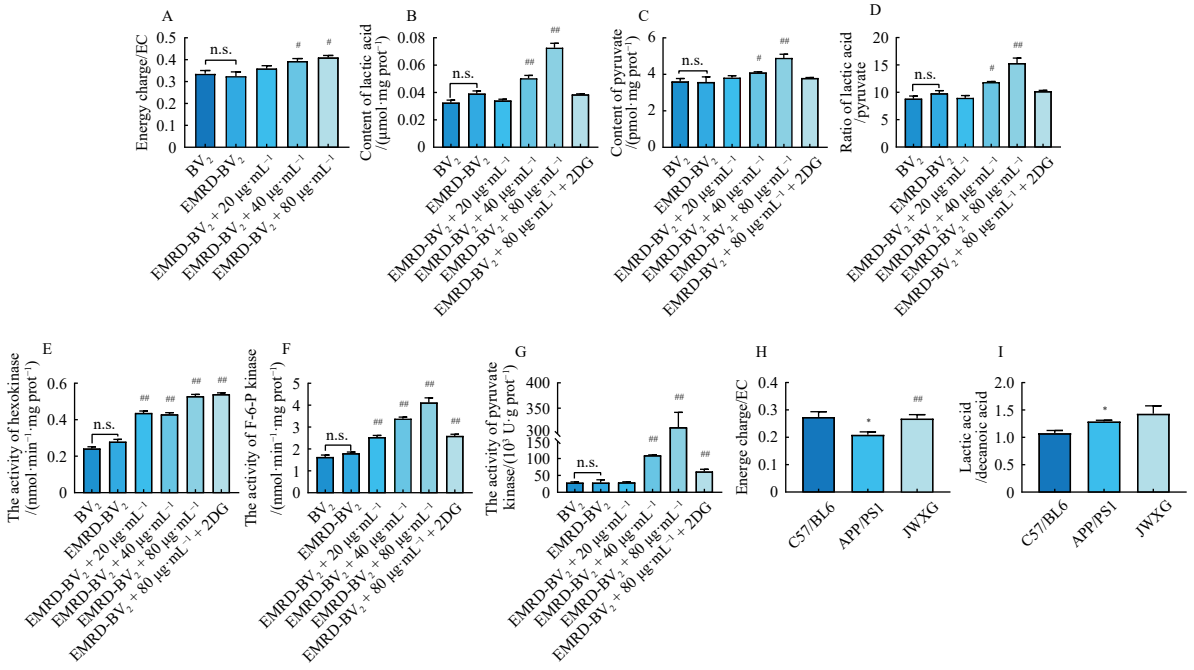

Fig. 3 JWXG increased energy production by enhancing EMR *in vitro* and *in vivo*. (A) The EC level in BV_2 cells (n = 6). (B, C) Levels of lactic acid and pyruvate in BV_2 cells (n = 6). (D) Lactic acid/pyruvate ratio in BV_2 cells (n = 6). (E–G) Activities of hexokinase, fructose-6-phosphate kinase and pyruvate kinase in BV_2 cells (n = 6). (H) EC levels of brain tissue in mice (n = 3). (I) Brain lactic acid levels in mice (n = 3). The data are expressed as mean ± SEM. $^{*}P < 0.05$ *vs* BV_2 cells or C57BL/6J mice; $^{\#}P < 0.05$, $^{\#\#}P < 0.01$ *vs* EMRD-BV_2 cells or APP/PS1 mice; n.s. means no significant differences.

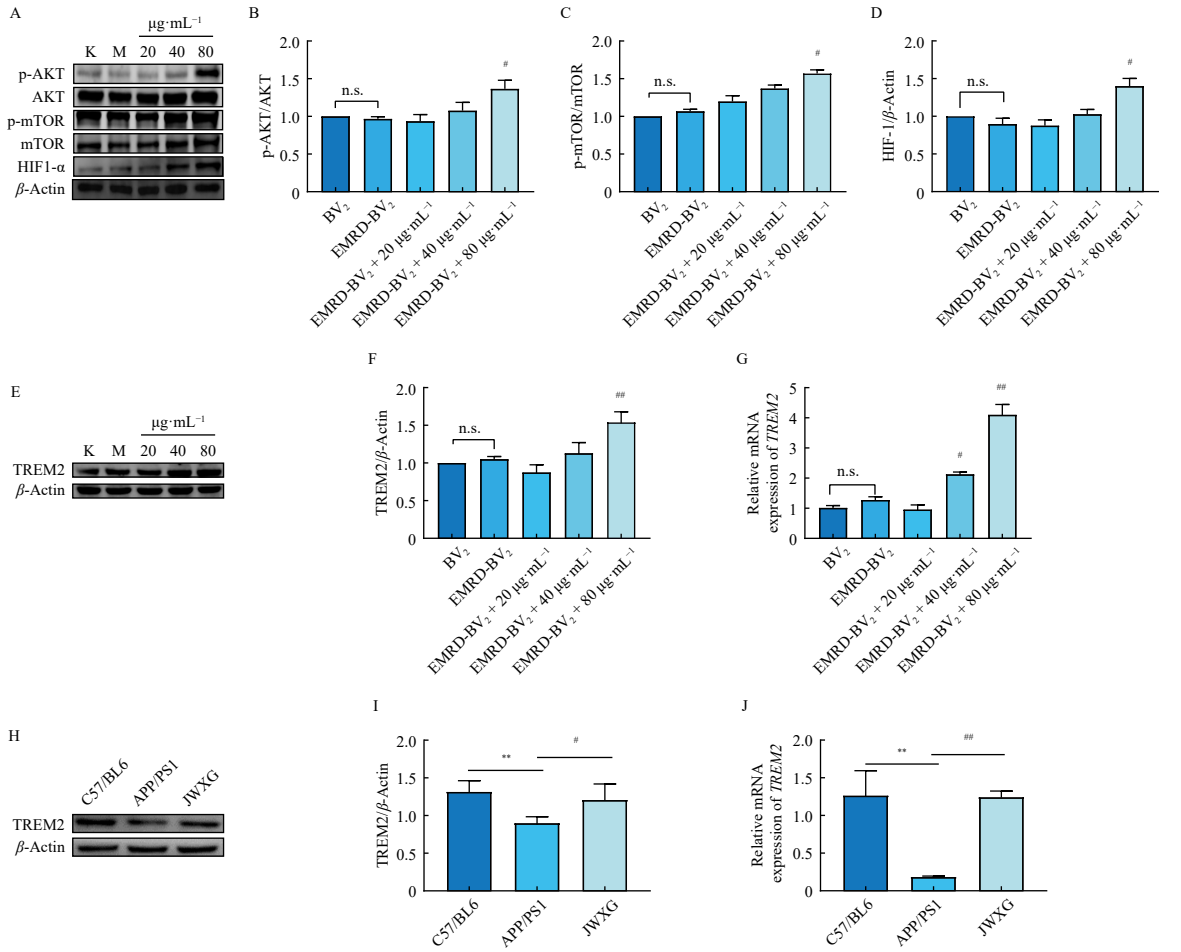

Fig. 4 JWXG activated TREM2-mediated Akt/mTOR/HIF-1α pathway. (A–D) Western blotting results of p-AKT/AKT, p-mTOR/mTOR, HIF-1α/β-actin *in vitro* (n = 6). (E, F) Western blotting results of TREM2 *in vitro* (n = 6). (G) *TREM2* mRNA expression *in vitro* (n = 6). (H, I) Western blotting results of TREM2 *in vivo* (n = 3). (J) *TREM2* mRNA expression *in vivo* (n = 3). The data are expressed as mean ± SEM. $^{**}P < 0.01$ *vs* BV_2 cells or C57BL/6J mice; $^{\#}P < 0.05$; $^{\#\#}P < 0.01$ *vs* EMRD-BV_2 cells or APP/PS1 mice; n.s. means no significant differences.

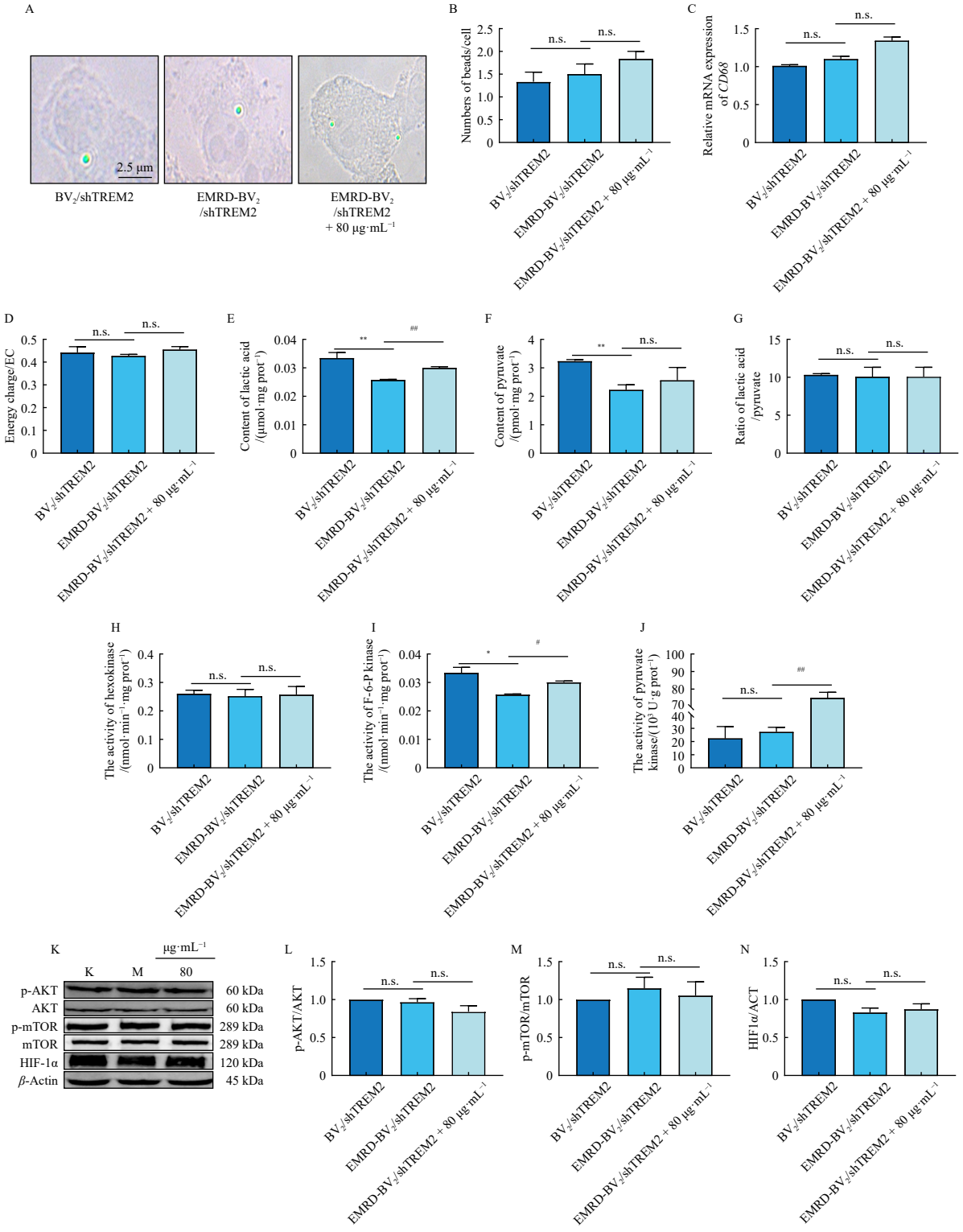

Fig. 5 shTREM2 partially reversed the effects of JWXG *in vitro*. (A) Representative images of the microglial phagocytosis of fluorescent latex beads *in vitro*. (B) Quantification of fluorescent latex beads per cell *in vitro*. (C) *CD68* mRNA levels *in vitro*. (D) EC levels *in vitro*. (E, F) Pyruvate and lactic acid levels *in vitro*. (G) Lactic acid/pyruvate ratio *in vitro*. (H–J). Activities of hexokinase, fructose-6-phosphate (F-6-P) kinase, and pyruvate kinase *in vitro*. (K–N) Representative images and quantitation of p-AKT/AKT, p-mTOR/mTOR, HIF-1α/*β*-actin *in vitro*. The data are expressed as mean ± SEM ($n = 6$). $^{*}P < 0.05$, $^{**}P < 0.01$ *vs* BV_2/shTREM2 cells; $^{\#}P < 0.05$, $^{\#\#}P < 0.01$ *vs* EMRD-BV_2/shTREM2 cells; n.s. means no significant differences.

al reduction and loss; however, JWXG treatment significantly mitigated these neuropathological changes (Fig. 7A). Additionally, JWXG administration significantly ameliorated the reduced $NeuN^{+}$ staining intensity in the CA1 and CA3 regions of APP/PS1 mice (Figs. 7B–Fig. 7D, $P < 0.05$ or $P < 0.01$). These findings further suggest that JWXG reduces Aβ burden and its neurotoxicity *in vivo* partially through enhanced microglial phagocytosis. The MWM test evaluated the mice's learning and memory capabilities. Escape latency, a critical MWM test indicator reflecting learning and memory ability, when prolonged, indicates impaired spatial learning and memory capacity [50]. As illustrated in Figs. 8A and 8B, mouse escape latency decreased progressively with increased training time ([4, 20] = 2.038). JWXG significantly reduced mouse escape latency compared to APP/PS1 mice ([4, 20] = 3.723).

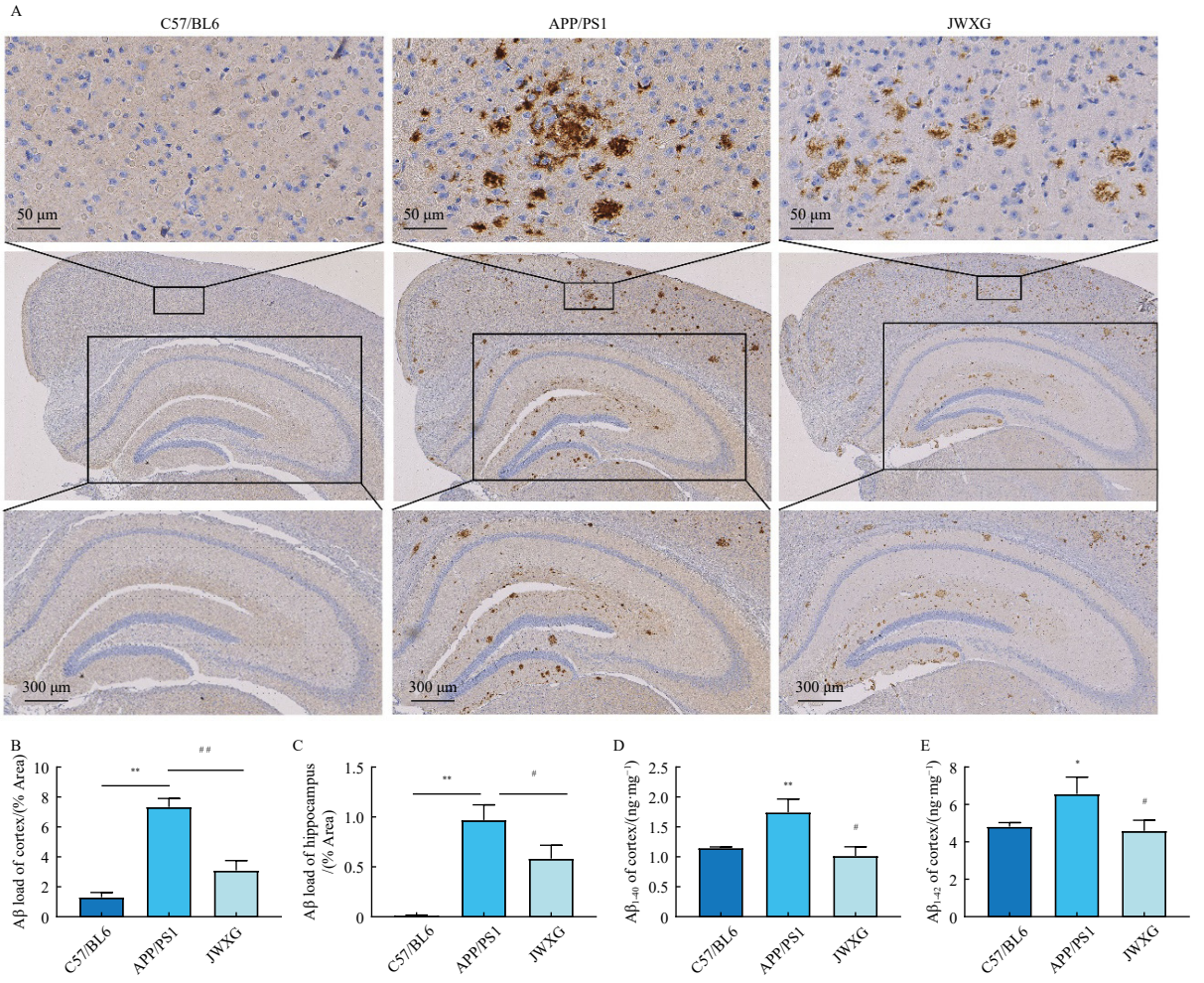

Fig. 6 JWXG reduced Aβ burden in APP/PS1 mice (n = 3). (A–C). Immunohistochemical staining and quantification of $A\beta^{+}$ plaques in the cerebral cortex and hippocampus of mice by immunohistochemistry staining (magnification: 200 × or 33 ×). (D, E). Levels of $A\beta_{1\text{-}40}$ and $A\beta_{1\text{-}42}$ of brain tissues *in vivo*. The data are expressed as mean ± SEM. $^{*}P$ < 0.05, $^{**}P$ < 0.01 *vs* C57BL/6J mice; $^{\#}P$ < 0.05, $^{\#\#}P$ < 0.01 *vs* APP/PS1 mice.

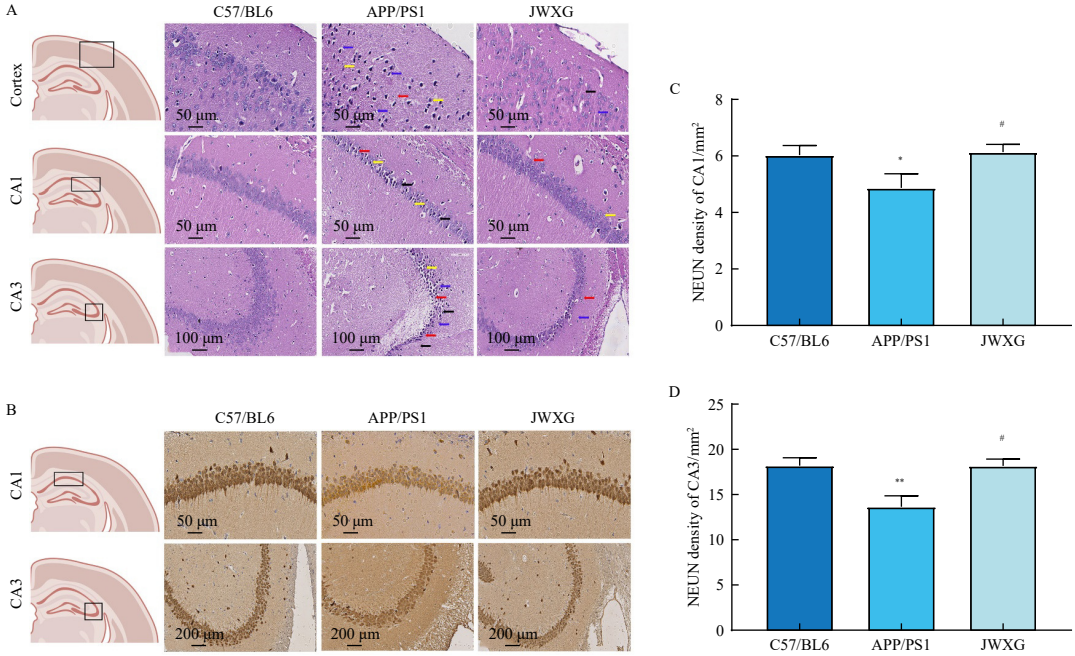

Fig. 7 JWXG attenuated the neuronal injury of APP/PS1 mice. (A) Representative images of H&E staining *in vivo* (magnification: 200 × or 100 ×); nerve cells scattered (red arrow), intercellular space enlarged (black arrow), nucleus staining deepened (yellow arrow), nucleus wrinkled (blue arrow). (B) Representative $NeuN^{+}$ images of immunohistochemical staining (magnification: 200 × or 50 ×). (C, D) $NeuN^{+}$ intensity of each group in CA1 and CA3 regions *in vivo*. The data are expressed as mean ± SEM (n = 3). $^{*}P$ < 0.05, $^{**}P$ < 0.01 *vs* C57BL/6J mice; $^{\#}P$ < 0.05 *vs* APP/PS1 mice.

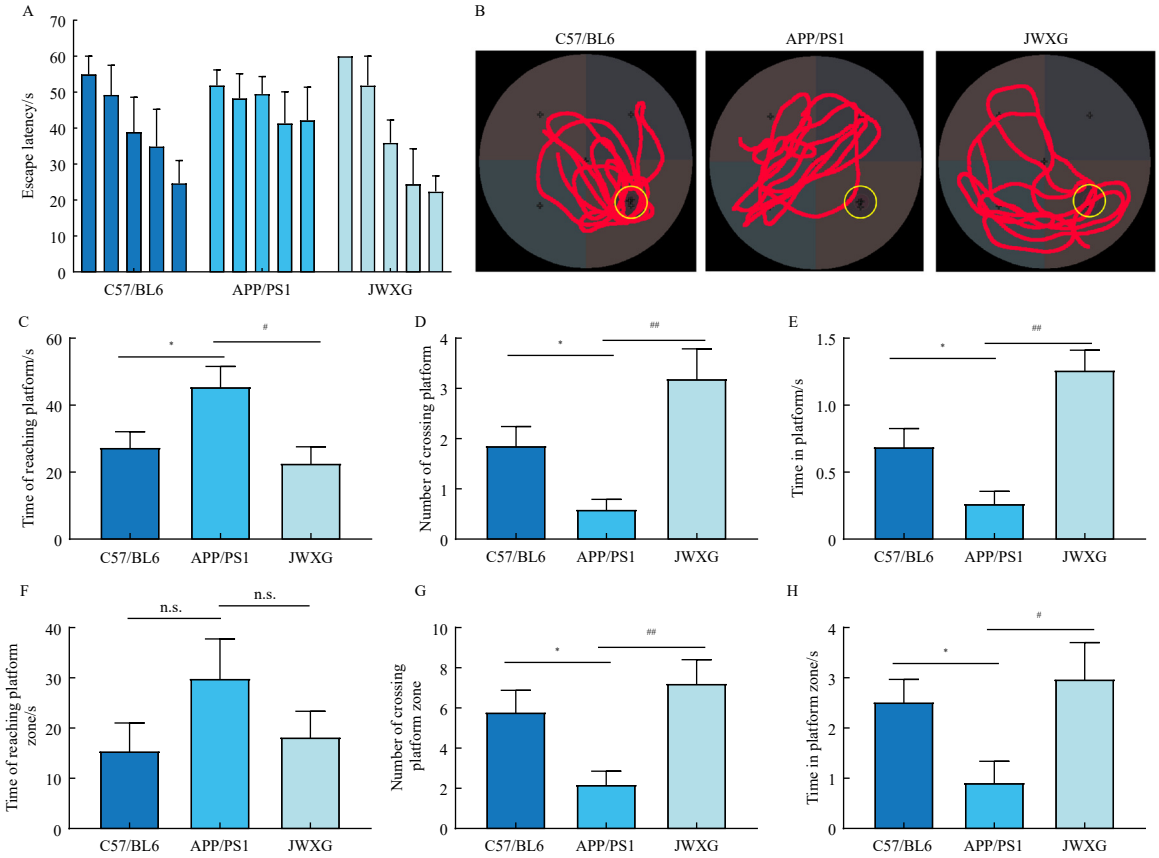

Fig. 8 JWXG ameliorated cognitive deficits in APP/PS1 mice. (A, B) Escape latency of mice and representative images of swimming tracks in the Morris water maze. (C) The time of reaching the platform. (D) Number of platform crossings. (E) Time spent on the platform. (F) Time to reach the platform zone. (G) Number of platform zone crossings. (H) The time spent in platform zone. The data are expressed as mean ± SEM (n = 3). $^{*}P < 0.05$ *vs* C57BL/6J mice; $^{\#}P < 0.05$, $^{\#\#}P < 0.01$ *vs* APP/PS1 mice.

APP/PS1 mice exhibited significantly diminished spatial learning abilities compared to the C57BL/6J group, demonstrated by increased platform and platform zone reaching time, decreased platform and platform zone crossing frequency, and reduced platform and platform zone dwelling time. However, JWXG treatment significantly reversed these alterations in JWXG mice compared to APP/PS1 mice (Figs. 8C–8H, $P < 0.05$ or $P < 0.01$).

4. Discussion

This study demonstrates that JWXG mitigated cognitive dysfunction and neuronal impairment in AD through activation of the TREM2/Akt/mTOR/HIF-1α pathway and enhancement of EMR to promote microglial phagocytosis. These findings suggest that enhancing EMR-mediated microglial phagocytosis may represent a promising therapeutic strategy for AD treatment.

Aβ accumulation and its associated neurotoxicity are considered primary contributors to AD pathogenesis, as they directly compromise cell membrane integrity and disrupt intracellular signaling pathways, leading to neuronal dysfunction or death [51-53]. Clinical evidence has demonstrated that removal of aggregated Aβ from brain tissue benefits AD patients [3], with FDA approval of two anti-amyloid antibodies, aducanumab and lecanemab, for AD treatment [54]. These developments confirm that facilitating Aβ clearance represents an effective therapeutic approach. Microglial phagocytosis, autophagy-lysosome pathway, and meningeal lymphatic system serve as crucial mechanisms for Aβ clearance and maintenance of brain homeostasis [55-57]. As central nervous system immune cells, microglia monitor the environment during injury response and maintain central homeostasis through phagocytosis and removal of toxic proteins, including Aβ [58-62]. During phagocytosis, microglia transform from a resting state to an amoeboid form, characterized by elevated *CD68* expression. Consequently, *CD68* mRNA serves as an established biomarker for microglial phagocytosis [63, 64]. Recent research emphasizes oAβ for their synaptic toxicity rather than fibrotic amyloid deposits, leading to the use of oAβ in EMRD-BV_2 cell studies [12, 65]. Our findings reveal significantly increased *CD68* mRNA expression and phagocytic fluorescent latex bead uptake in oAβ acute stimulation-induced BV_2 cells, while no significant differences were observed between immune-tolerant BV_2 cells induced by oAβ repeated stimulation (EMRD-BV_2) and unstimulated-BV_2 cells. Similarly, microglial Aβ phagocytosis showed marked deficits in 9-mo APP/PS1 mice. Notably, JWXG significantly enhanced *CD68* mRNA expression and microglial phagocytosis in both EMRD-BV_2 cells and 9-mo APP/PS1 mice, demonstrating its efficacy in promoting microglial phagocytosis *in vitro* and *in vivo*.

Microglia perform diverse functions that require varying levels of energy, with their metabolic pathways adapting accordingly [12]. In a resting state, glucose metabolism primarily occurs through OXPHOS, but when stimulated by neurotoxic substances such as Aβ or cellular debris, the microglial energy supply shifts from OXPHOS to aerobic glycolysis [66]. Although less efficient in ATP generation compared with mitochondrial respiration, glycolysis enables a faster rate of glucose metabolism, essential for energy-demanding processes like phagocytosis [14]. Research indicates that disruption in EMR leads to microglial dysfunction in AD, demonstrating a strong connection between EMR and phagocytosis [12]. Recent studies have demonstrated that myeloid cell dysfunction can be reversed by reprogramming myeloid glucose metabolism to restore youthful immune functions and cognitive abilities [67, 68]. This evidence suggests that EMR is crucial for microglial phagocytosis. HK, F-6-PK, and PK serve as three rate-limiting enzymes of glycolysis, while lactic acid levels and the lactic acid/pyruvate ratio typically indicate glucose metabolism status [69, 70]. Our data revealed that JWXG treatment increased EC,

lactic acid content, and lactic acid/pyruvate ratio in EMRD-BV_2 cells, along with a dose-dependent increase in glycolysis rate-limiting enzyme activity. 2-DG, a glucose analog and HK substrate, inhibits glycolysis by reducing HK product rather than HK activity. As anticipated, 2-DG reversed JWXG's effects on glycolysis rate-limiting enzyme activity (except for HK). The enhanced glycolysis levels significantly correlated with increased *CD68* expression and phagocytosis both *in vitro* and *in vivo*. These results indicate that JWXG enhances microglial phagocytic function through EMR promotion.

The Akt/mTOR/HIF-1α pathway serves a critical role in inducing aerobic glycolysis and EMR [15, 71, 72]. Multiple studies demonstrate that JWXG's active ingredients, including baicalin [73], baicalein [74], ferulic acid [75], and chlorogenic acid [33], can activate the Akt/mTOR pathway, suggesting JWXG may enhance EMR through increased Akt/mTOR/HIF-1α pathway activity. Our findings revealed that JWXG significantly activated the Akt/mTOR/HIF-1α pathway in EMRD-BV_2 cells and 9-mo APP/PS1 mice. These results suggest JWXG's enhancement of microglial phagocytosis closely relates to Akt/mTOR/HIF-1α pathway activation. TREM2, a transmembrane glycoprotein specifically expressed in CNS microglia, has loss-of-function mutations widely considered a high-risk factor for late-onset AD [76, 77]. Furthermore, TREM2 is essential for microglial phagocytosis and maintains cellular energetic and biosynthetic metabolism during AD [9, 78]. TREM2 agonist antibodies are currently under investigation for AD treatment in preclinical trials [79]. Aβ, a TREM2 ligand, directly binds to TREM2's extracellular domain, resulting in mTOR phosphorylation and HIF-1α activation, thereby initiating EMR [17-19, 80, 81]. Additionally, baicalin promotes TREM2 levels in microglia [82]. Our results demonstrated significantly decreased TREM2 gene and protein expression in APP/PS1 mice and EMRD-BV_2 cells, which JWXG treatment notably restored. Notably, shTREM2 blockade of TREM2 in EMRD-BV2 cells partially reversed JWXG's effects on microglial phagocytosis, glycolysis-mediated energy production, and Akt/mTOR/HIF-1α pathway activation. Finally, our data demonstrated that JWXG significantly reduced Aβ burden and neuronal impairment in the cortex and hippocampus while alleviating cognitive deficits in 9-mo APP/PS1 mice. These findings suggest JWXG attenuates cognitive deficits in APP/PS1 mice by activating TREM2-mediated Akt/mTOR/HIF-1α pathway facilitated microglial phagocytosis.

Funding

This work was supported by the National Natural Science Foundation of China (Nos. 82074150 and 82274240) and the Natural Science Foundation of Sichuan Province (No. 2023NSFSC1779).

Declaration of competing interest

These authors have no conflict of interest to declare.

References

1 van Dyck CH, Swanson CJ, Aisen P, et al. Lecanemab in early Alzheimer's disease. *N Engl J Med*. 2023;388(1):9-21. https://doi.org/10.1056/NEJMoa2212948.
2 Bassil F, Brown HJ, Pattabhiraman S, et al. Amyloid-beta (Aβ) plaques promote seeding and spreading of α-synuclein and tau in a mouse model of lewy body disorders with Aβ pathology. *Neuron*. 2020;105(2):260-275.e6. https://doi.org/10.1016/j.neuron.2023.10.030.
3 Jucker M, Walker LC. Alzheimer's disease: from immunotherapy to immunoprevention. *Cell*. 2023;186(20):4260-4270. https://doi.org/10.1016/j.cell.2023.08.021.
4 Evans CD, Sparks J, Andersen SW, et al. APOE ε4's impact on response to amyloid therapies in early symptomatic Alzheimer's disease: analyses from multiple clinical trials. *Alzheimers Dement*. 2023;19(12):5407-5417. https://doi.org/10.1002/alz.13128.
5 Cummings J, Apostolova L, Rabinovici GD, et al. Lecanemab: appropriate use recommendations. *J Prev Alzheimers Dis*. 2023;10(3):362-377. https://doi.org/10.14283/jpad.2023.30.
6 Söderberg L, Johannesson M, Nygren P, et al. Lecanemab, aducanumab, and gantenerumab-binding profiles to different forms of amyloid-β might explain efficacy and side effects in clinical trials for Alzheimer's disease. *Neurotherapeutics*. 2023;20(1):195-206. https://doi.org/10.1007/s13311-022-01308-6.
7 Grubman A, Choo XY, Chew G, et al. Transcriptional signature in microglia associated with Aβ plaque phagocytosis. *Nat Commun*. 2021;12(1):3015. https://doi.org/10.1038/s41467-021-23111-1.
8 Parhizkar S, Gent G, Chen Y, et al. Sleep deprivation exacerbates microglial reactivity and Aβ deposition in a TREM2-dependent manner in mice. *Sci Transl Med*. 2023;15(693):eade6285. https://doi.org/10.1126/scitranslmed.ade6285.
9 Ulland TK, Song WM, Huang SC, et al. TREM2 maintains mmicroglial metabolic fitness in Alzheimer's disease. *Cell*. 2017;170(4):649-663.e13. https://doi.org/10.1016/j.cell.2017.07.023.
10 Li L, Chen Q, Qin Y, et al. Regulation of TREM2 on BV_2 inflammation through PI3K/AKT/mTOR pathway. *Biotechnol Genet Eng Rev*. 2024;40(4):4040-4061. https://doi.org/10.1080/02648725.2023.2204719.
11 Shi Q, Chang C, Saliba A, et al. Microglial mTOR activation upregulates TREM2 and enhances β-amyloid plaque clearance in the 5XFAD Alzheimer's disease model. *J Neurosci*. 2022;42(27):5294-5313. https://doi.org/10.1523/JNEUROSCI.2427-21.2022.
12 Baik SH, Kang S, Lee W, et al. A breakdown in metabolic reprogramming causes microglia dysfunction in Alzheimer's disease. *Cell Metab*. 2019;30(3):493-507.e6. https://doi.org/10.1016/j.cmet.2019.06.005.
13 Liu J, Feng R, Wang D, et al. Triclosan-induced glycolysis drives inflammatory activation in microglia *via* the Akt/mTOR/HIF 1α signaling pathway. *Ecotoxicol Environ Saf*. 2021;224:112664. https://doi.org/10.1016/j.ecoenv.2021.112664.
14 Breda CNS, Davanzo GG, Basso PJ, et al. Mitochondria as central hub of the immune system. *Redox Biol*. 2019;26:101255. https://doi.org/10.1016/j.redox.2019.101255.
15 Lu J, Wang C, Cheng X, et al. A breakdown in microglial metabolic reprogramming causes internalization dysfunction of α-synuclein in a mouse model of Parkinson's disease. *J Neuroinflammation*. 2022;19(1):113. https://doi.org/10.1186/s12974-022-02484-0.
16 Lu J, Zhou W, Dou F, et al. TRPV1 sustains microglial metabolic reprogramming in Alzheimer's disease. *EMBO Rep*. 2021;22(6):e52013. https://doi.org/10.15252/embr.202052013.
17 Huang Y, Happonen KE, Burrola PG, et al. Microglia use TAM receptors to detect and engulf amyloid β plaques. *Nat Immunol*. 2021;22(5):586-594. https://doi.org/10.1038/s41590-021-00913-5.
18 Zhao P, Xu Y, Jiang L, et al. A tetravalent TREM2 agonistic antibody reduced amyloid pathology in a mouse model of Alzheimer's disease. *Sci Transl Med*. 2022;14(661):eabq0095. https://doi.org/10.1126/scitranslmed.abq0095.
19 Zhao N, Bu G. A TREM2 antibody energizes microglia. *Nat Neurosci*. 2023;26(3):366-368. https://doi.org/10.1038/s41593-023-01265-z.
20 Han X, Xu T, Fang Q, et al. Quercetin hinders microglial activation to alleviate neurotoxicity *via* the interplay between NLRP3 inflammasome and mitophagy. *Redox Biol*. 2021;44:102010. https://doi.org/10.1016/j.redox.2021.102010.
21 Li N, Yan X, Huang W, et al. Curcumin protects against the age-related hearing loss by attenuating apoptosis and senescence *via* activating Nrf2 signaling in cochlear hair cells. *Biochem Pharmacol*. 2023;212:115575. https://doi.org/10.1016/j.bcp.2023.115575.
22 Fernandes F, Barroso MF, De Simone A, et al. Multi-target neuroprotective effects of herbal medicines for Alzheimer's disease. *J Ethnopharmacol*. 2022;290:115107. https://doi.org/10.1016/j.jep.2022.115107.
23 Ospondpant D, Xia Y, Lai QWS, et al. The extracts of *Dracaena cochinchinensis* stemwood suppress inflammatory response and phagocytosis in lipopolysaccharide-activated microglial cells. *Phytomedicine*. 2023;118:154936. https://doi.org/10.1016/j.phymed.2023.154936.
24 Liu H, Wang J, Sekiyama A, et al. Juzen-Taiho-To, an herbal medicine, activates and enhances phagocytosis in microglia/macrophages. *Tohoku J Exp Med*. 2008;215(1):43-54. https://doi.org/10.1620/tjem.215.43.
25 Li P, Huang FK, Yang C, et al. Advance in studies on traditional Chinese medicine on Aβ's scavenging effect. *Chin J Chin Mater Med*. 2013;38(23):4020-4023. https://doi.org/10.4268/cjcmm20132305.
26 Wei J, Fu W, Chen H, et al. Tongluo Xingnao effervescent tablets ameliorates cognitive function of SAMP8 mice *via* Nampt/SIRT1/FOXO3 pathway. *Chin Tradit Pat Med*. 2017;39(4):684-689. https://doi.org/10.3969/j.issn.1001-1528.2017.04.00.
27 Dai Y, Ma T, Ren X, et al. Tongluo Xingnao effervescent tablet preserves mitochondrial energy metabolism and attenuates cognition deficits in APPswe/PS1De9 mice. *Neurosci Lett*. 2016;630:101-108. https://doi.org/10.1016/j.neulet.2016.07.044.
28 Fu WJ. *Studies on the Effect of Tongluoxingnao Effervescent Tablet on Aβ Metabolism in Transgenic AD Models*. Chendu Universtiy of TCM, 2017.
29 Hu Y, Ju SH, Zhang YJ, et al. Effect of Tongluo Xingnao effervescent tablets on learning and memory dysfunction in rats with chronic cerebral ischemia. *Chin J Chin Mater Med*. 2014;39(10):1908-1912. https://doi.org/10.4268/cjcmm20141029.
30 Zhang YJ, Dai Y, Hu Y, et al. Effect of Tongluo Xingnao effervescent tablet on learning and memory of AD rats and expression of insulin-degrading enzyme in hippocampus. *Chin J Chin Mater Med*. 2013;38(17):2863-2867. https://doi.org/mdl-24380312.
31 Fu WJ, Yuan D, Tao M, et al. Tongluo Xingnao effervescent tablet reverses memory deficit and reduces plaque load in APPswe/PS1dE9 mice. *Exp Ther Med*. 2018;15(4):4005-4013. https://doi.org/10.3892/etm.2018.5897.
32 Hu Y. *Studies on the Effect of Tongluoxingnao Effervescent Tablet on Brain Energy Metabolism in Multi-infarct Dementia Rats*. Chendu Universtiy of TCM, 2015.
33 Li J, Chen X, Li X, et al. Cryptochlorogenic acid and its metabolites ameliorate myocardial hypertrophy through a HIF1α-related pathway. *Food Funct*. 2022;13(4):2269-2282. https://doi.org/10.1039/D1FO03838A.
34 Yang J, Jia Z, Xiao Z, et al. Baicalin rescues cognitive dysfunction, mitigates neurodegeneration, and exerts anti-epileptic effects through activating TLR4/

MYD88/Caspase-3 pathway in rats. *Drug Des Devel Ther*. 2021;15:3163-3180. https://doi.org/10.2147/DDDT.S314076.
35 Jin X, Liu MY, Zhang DF, et al. Baicalin mitigates cognitive impairment and protects neurons from microglia-mediated neuroinflammation *via* suppressing NLRP3 inflammasomes and TLR4/NF-κB signaling pathway. *CNS Neurosci Ther*. 2019;25(5):575-590. https://doi.org/10.1111/cns.13086.
36 Li Z, Zheng G, Wang N, et al. A Flower-like brain targeted selenium nanocluster lowers the chlorogenic acid dose for ameliorating cognitive impairment in APP/PS1 mice. *J Agric Food Chem*. 2023;71(6):2883-2897. https://doi.org/10.1021/acs.jafc.2c06809.
37 Shi D, Hao Z, Qi W, et al. Aerobic exercise combined with chlorogenic acid exerts neuroprotective effects and reverses cognitive decline in Alzheimer's disease model mice (APP/PS1) *via* the SIRT1/PGC-1α/PPARγ signaling pathway. *Front Aging Neurosci*. 2023;15:1269952. https://doi.org/10.3389/fnagi.2023.1269952.
38 Mahaman YAR, Huang F, Salissou MTM, et al. Ferulic acid improves synaptic plasticity and cognitive impairments by alleviating the PP2B/DARPP-32/PP1 axis-mediated STEP increase and Aβ burden in Alzheimer's disease. *Neurotherapeutics*. 2023;20(4):1081-1108. https://doi.org/10.1007/s13311-023-01356-6.
39 Shi J, Chen J, Xie X, et al. Baicalein-corrected gut microbiota may underlie the amelioration of memory and cognitive deficits in APP/PS1 mice. *Front Pharmacol*. 2023;14:1132857. https://doi.org/10.3389/fphar.2023.1132857.
40 Cai Q, Li Y, Pei G. Polysaccharides from *Ganoderma lucidum* attenuate microglia-mediated neuroinflammation and modulate microglial phagocytosis and behavioural response. *J Neuroinflammation*. 2017;14(1):63. https://doi.org/10.1186/s12974-017-0839-0.
41 Chen Y, Yang C, Zou M, et al. Inhibiting mitochondrial inflammation through Drp1/HK1/NLRP3 pathway: a mechanism of alpinetin attenuated aging-associated cognitive impairment. *Phytother Res*. 2023;37(6):2454-2471. https://doi.org/10.1002/ptr.7767.
42 Zhan M, Liu X, Xia X, et al. Promotion of neuroinflammation by the glymphatic system: a new insight into ethanol extracts from *Alisma orientale* in alleviating obesity-associated cognitive impairment. *Phytomedicine*. 2024;122:155147. https://doi.org/10.1016/j.phymed.2023.155147.
43 Yang C, Lu L, Liao L, et al. Establishment of GC-MS method for the determination of *Pseudomonas aeruginosa* biofilm and its application in metabolite enrichment analysis. *J Chromatogr B Analyt Technol Biomed Life Sci*. 2021;1179:122839. https://doi.org/10.1016/j.jchromb.2021.122839.
44 Wang Y, Cella M, Mallinson K, et al. TREM2 lipid sensing sustains the microglial response in an Alzheimer's disease model. *Cell*. 2015;160(6):1061-1071. https://doi.org/10.1016/j.cell.2015.01.049.
45 Kapogiannis D, Mattson MP. Disrupted energy metabolism and neuronal circuit dysfunction in cognitive impairment and Alzheimer's disease. *Lancet Neurol*. 2011;10(2):187-198. https://doi.org/10.1016/S1474-4422(10)70277-5.
46 Cunnane SC, Trushina E, Morland C, et al. Brain energy rescue: an emerging therapeutic concept for neurodegenerative disorders of ageing. *Nat Rev Drug Discov*. 2020;19(9):609-633. https://doi.org/10.1038/s41573-020-0072-x.
47 Terada T, Obi T, Bunai T, et al . *In vivo* mitochondrial and glycolytic impairments in patients with Alzheimer disease. *Neurology*. 2020;94(15):e1592-e1604. https://doi.org/10.1212/WNL.0000000000009249.
48 Fairley LH, Lai KO, Wong JH, et al. Mitochondrial control of microglial phagocytosis by the translocator protein and hexokinase 2 in Alzheimer's disease. *Proc Natl Acad Sci U S A*. 2023;120(8):e2209177120. https://doi.org/10.1073/pnas.2209177120.
49 Sowade RF, Jahn TR. Seed-induced acceleration of amyloid-β mediated neurotoxicity *in vivo*. *Nat Commun*. 2017;8(1):512. https://doi.org/10.1038/s41467-017-00579-4.
50 Hernández-Mercado K, Zepeda A. Morris water maze and contextual fear conditioning tasks to evaluate cognitive functions associated with adult hippocampal neurogenesis. *Front Neurosci*. 2021;15:782947. https://doi.org/10.3389/fnins.2021.782947.
51 Darling AL, Shorter J. Atomic structures of amyloid-β oligomers illuminate a neurotoxic mechanism. *Trends Neurosci*. 2020;43(10):740-743. https://doi.org/10.1016/j.tins.2020.07.006.
52 Puntambekar SS, Moutinho M, Lin PB, et al. CX3CR1 deficiency aggravates amyloid driven neuronal pathology and cognitive decline in Alzheimer's disease. *Mol Neurodegener*. 2022;17(1):47. https://doi.org/10.1186/s13024-022-00545-9.
53 Wen W, Li P, Liu P, et al. Post-translational modifications of BACE1 in Alzheimer's disease. *Curr Neuropharmacol*. 2022;20(1):211-222. https://doi.org/10.2174/1570159X19666210121163224.
54 Høilund-Carlsen PF, Revheim ME, Costa T, et al. Passive Alzheimer's immunotherapy: a promising or uncertain option? *Ageing Res Rev*. 2023;90:101996. https://doi.org/10.1016/j.arr.2023.101996.
55 Xin SH, Tan L, Cao X, et al. Clearance of amyloid β and Tau in Alzheimer's disease: from mechanisms to therapy. *Neurotox Res*. 2018;34(3):733-748. https://doi.org/10.1007/s12640-018-9895-1.
56 Da Mesquita S, Louveau A, Vaccari A, et al. Functional aspects of meningeal lymphatics in ageing and Alzheimer's disease. *Nature*. 2018;560(7717):185-191. https://doi.org/10.1038/s41586-018-0368-8.
57 Vilchez D, Saez I, Dillin A . The role of protein clearance mechanisms in organismal ageing and age-related diseases. *Nat Commun*. 2014;5:5659. https://doi.org/10.1038/ncomms6659.
58 Bhattacherjee A, Jung J, Zia S, et al. The CD33 short isoform is a gain-of-function variant that enhances $A\beta_{1-42}$ phagocytosis in microglia. *Mol Neurodegener*. 2021;16(1):19. https://doi.org/10.1186/s13024-021-00443-6.
59 Arcuri C, Mecca C, Bianchi E, et al. The pathophysiological role of microglia in dynamic surveillance, phagocytosis and structural remodeling of the developing CNS. *Front Mol Neurosci*. 2017;10:191. https://doi.org/10.3389/fnmol.2017.00191.
60 Villacampa N, Heneka MT. Microglia in Alzheimer's disease: local heroes! *J Exp Med*. 2020;217(4):e20192311. https://doi.org/10.1084/jem.20192311.
61 Cserép C, Pósfai B, Lénárt N, et al. Microglia monitor and protect neuronal function through specialized somatic purinergic junctions. *Science*. 2020;367(6477):528-537. https://doi.org/10.1126/science.aax6752.
62 Gao C, Jiang J, Tan Y, et al. Microglia in neurodegenerative diseases: mechanism and potential therapeutic targets. *Signal Transduct Target Ther*. 2023;8(1):359. https://doi.org/10.1038/s41392-023-01588-0.
63 Bassett B, Subramaniyam S, Fan Y, et al. Minocycline alleviates depression-like symptoms by rescuing decrease in neurogenesis in dorsal hippocampus *via* blocking microglia activation/phagocytosis. *Brain Behav Immun*. 2021;91:519-530. https://doi.org/10.1016/j.bbi.2020.11.009.
64 Lecours C, St-Pierre MK, Picard K, et al. Levodopa partially rescues microglial numerical, morphological, and phagolysosomal alterations in a monkey model of Parkinson's disease. *Brain Behav Immun*. 2020;90:81-96. https://doi.org/10.1016/j.bbi.2020.07.044.
65 Ashe KH. The biogenesis and biology of amyloid β oligomers in the brain. *Alzheimers Dement*. 2020;16(11):1561-1567. https://doi.org/10.1002/alz.12084.
66 Glass CK, Natoli G. Molecular control of activation and priming in macrophages. *Nat Immunol*. 2016;17(1):26-33. https://doi.org/10.1038/ni.3306.
67 Minhas PS, Latif-Hernandez A, McReynolds MR, et al. Restoring metabolism of myeloid cells reverses cognitive decline in ageing. *Nature*. 2021;590(7844):122-128. https://doi.org/10.1038/s41586-020-03160-0.
68 Li W, Wang S, Zhang H, et al. Honokiol restores microglial phagocytosis by reversing metabolic reprogramming. *J Alzheimers Dis*. 2021;82(4):1475-1485. https://doi.org/10.3233/JAD-210177.
69 Patgiri A, Skinner OS, Miyazaki Y, et al. An engineered enzyme that targets circulating lactate to alleviate intracellular NADH∶NAD$^+$ imbalance. *Nat Biotechnol*. 2020;38(3):309-313. https://doi.org/10.1038/s41587-019-0377-7.
70 Pan RY, He L, Zhang J, et al. Positive feedback regulation of microglial glucose metabolism by histone H4 lysine 12 lactylation in Alzheimer's disease. *Cell Metab*. 2022;34(4):634-648.e6. https://doi.org/10.1016/j.cmet.2022.02.013.
71 Cheng SC, Quintin J, Cramer RA, et al. mTOR- and HIF-1α-mediated aerobic glycolysis as metabolic basis for trained immunity. *Science*. 2014;345(6204):1250684. https://doi.org/10.1126/science.1250684.
72 Yang F, Zhao D, Cheng M, et al. mTOR-mediated immunometabolic reprogramming nanomodulators enable sensitive switching of energy deprivation-induced microglial polarization for Alzheimer's disease management. *ACS Nano*. 2023;17(16):15724-15741. https://doi.org/10.1021/acsnano.3c03232.
73 Zhu Y, Fang J, Wang H, et al. Baicalin suppresses proliferation, migration, and invasion in human glioblastoma cells *via* Ca^{2+}-dependent pathway. *Drug Des Devel Ther*. 2018;12:3247-3261. https://doi.org/10.2147/DDDT.S176403.
74 Li P, Hu J, Shi B, et al. Baicalein enhanced cisplatin sensitivity of gastric cancer cells by inducing cell apoptosis and autophagy *via* Akt/mTOR and Nrf2/Keap 1 pathway. *Biochem Biophys Res Commun*. 2020;531(3):320-327. https://doi.org/10.1016/j.bbrc.2020.07.045.
75 Cheng CY, Kao ST, Lee YC. Ferulic acid ameliorates cerebral infarction by activating Akt/mTOR/4E-BP1/Bcl-2 anti-apoptotic signaling in the penumbral cortex following permanent cerebral ischemia in rats. *Mol Med Rep*. 2019;19(2):792-804. https://doi.org/10.3892/mmr.2018.9737.
76 Hou J, Chen Y, Grajales-Reyes G, et al. TREM2 dependent and independent functions of microglia in Alzheimer's disease. *Mol Neurodegener*. 2022;17(1):84. https://doi.org/10.1186/s13024-022-00588-y.
77 Griciuc A, Patel S, Federico AN, et al. TREM2 acts downstream of CD33 in modulating microglial pathology in Alzheimer's disease. *Neuron*. 2019;103(5):820-835.e7. https://doi.org/10.1016/j.neuron.2019.06.010.
78 Zhou Y, Song WM, Andhey PS, et al. Human and mouse single-nucleus transcriptomics reveal TREM2-dependent and TREM2-independent cellular responses in Alzheimer's disease. *Nat Med*. 2020;26(1):131-142. https://doi.org/10.1038/s41591-019-0695-9.
79 Schlepckow K, Morenas-Rodríguez E, Hong S, et al. Stimulation of TREM2 with agonistic antibodies-an emerging therapeutic option for Alzheimer's disease. *Lancet Neurol*. 2023;22(11):1048-1060. https://doi.org/10.1016/S1474-4422(23)00247-8.
80 Xu Q, Xu W, Cheng H, et al. Efficacy and mechanism of cGAMP to suppress Alzheimer's disease by elevating TREM2. *Brain Behav Immun*. 2019;81:495-508. https://doi.org/10.1016/j.bbi.2019.07.004.
81 Manrique-Castano D, Dzyubenko E, Borbor M, et al. Tenascin-C preserves microglia surveillance and restricts leukocyte and, more specifically, T cell infiltration of the ischemic brain. *Brain Behav Immun*. 2021;91:639-648. https://doi.org/10.1016/j.bbi.2020.10.016.
82 Wang H, Ma J, Li X, et al. FDA compound library screening baicalin upregulates TREM2 for the treatment of cerebral ischemia-reperfusion injury. *Eur J Pharmacol*. 2024;969:176427. https://doi.org/10.1016/j.ejphar.2024.176427.